Iterative reconstruction method for three-dimensional optoacoustic imaging

G. Paltauf[*a], J.A. Viator[b], S.A. Prahl[b], S.L. Jacques[b]

[a]Institut fuer Experimentalphysik, Karl-Franzens-Universitaet Graz, Austria

[b]Oregon Medical Laser Center, Portland, Oregon

ABSTRACT

Three-dimensional optoacoustic imaging uses detection of laser-generated thermoelastic waves with an ultrasound sensor array. Integrated acoustic signals (velocity potentials) are back projected into the source volume to give a map of absorbed laser energy. Since the number of array elements and the receiving solid angle are limited, radial back projection produces artifacts such as back projection arcs. To solve this problem, we developed in this study an iterative method for image reconstruction. A first image estimate was generated by simple radial back projection. A model for signal generation from a volume containing arbitrary optoacoustic sources was then used to calculate acoustic wave propagation from this estimate. Calculated signals at the array elements were compared with the measured signals and the difference was used to improve the image. In simulations and experiments we used the algorithm to obtain three-dimensional images of multiple optoacoustic sources. With signals from an array of 3 x 3 detector elements a significant improvement was observed after about 10 iterations compared to the simple radial back projection. Although computationally more intensive, iterative reconstruction can minimize the time and instrumentation for signal acquisition because a small number of array elements already gives a good quality of the optoacoustic image.

Keywords: photoacoustic, thermoacoustic, thermoelastic, inverse problems, deconvolution

1. INTRODUCTION

Optoacoustic or thermoacoustic imaging is based on the generation of acoustic waves by heating a sample with a short pulse of electromagnetic radiation in the visible, infrared or microwave range. The mechanism that causes the acoustic wave is the thermoelastic effect. Heating and subsequent thermal expansion of an optically absorbing structure cause a disturbance that propagates from its source with the speed of sound. The initial thermoelastic stress that is generated in the heated structure is maximized if the duration of the laser pulse, t_p, is shorter than the acoustic relaxation time, $t_{ac} = d/c$, where d is the characteristic size of the heated volume. Under this condition, commonly called stress confinement, the acoustic wave solely depends on properties of the absorbing structure such as size, shape, optical and thermal properties. The temporal profile and the arrival time of signals detected at the elements of an ultrasound detector array outside the sample are used to reconstruct an image of the distribution of absorbed energy. The methods and algorithms to accomplish this reconstruction are based on some kind of back projection of signals [1-4], distributing pressure or some derived quantity over all possible source locations. Optoacoustic image reconstruction is related to x-ray computer tomography (CT), where the information acquired with a scanning or array detector represents the two-or three-dimensional Radon transform that is back projected to create a section or volume image of the object. This similarity has led to reconstruction methods for optoacoustic imaging that are based on inverse Radon transforms [5]. The difference is that the Radon transform represents projections along straight lines or planes, whereas the optoacoustic signal at a given time is the integral over a spherical surface. Due to the integration there exists a principal ambiguity in the reconstruction. Back projecting a signal from a point source that is detected with an isotropic sensor gives a spherical surface in the reconstruction. Only with a sufficient number of detectors that measure signals from many directions the superposition of back projections gives the accurate position of the source. In x-ray CT projections from all directions are used to acquire the information for a section image. This is usually done by rotating the x-ray source and the detector 360 degrees around the imaged object. Back projection and filtering creates an image with very few artifacts.

[*] Correspondence: E-mail: guenther.paltauf@kfunigraz.ac.at

G. Paltaulf, J. A. Viator, S. A. Prahl, S. L. Jacques, “Iterative reconstruction method for three-dimensional optoacoustic imaging,” in *SPIE Proceedings of Biomedical Optoacoustics*, A. A. Oraevsky, **4256**, pp. 138–146, (2001).

There are two major difficulties in optoacoustic imaging when compared to x-ray CT. First of all optoacoustic imaging is always a three-dimensional problem. Signal generation cannot be limited to a thin section as with collimated x-rays because optical radiation is strongly scattered in tissue. Complete data acquisition should therefore take place in the full 4π solid angle around the object. The second difficulty is the fact that signal generation is limited to depths to which light can penetrate, that is to several mm or a few cm, depending on wavelength. Acoustic wave propagation distances are also limited due to the frequency-dependent attenuation of sound. These limitations allow to acquire signals only from a limited solid angle around the object. For example, for thermoacoustic breast imaging curved detector arrays have been investigated that cover nearly a 2π solid angle [3]. For other applications, however, plane arrays have to be used that are in contact with the tissue surface and cover a smaller solid angle. Incomplete data acquisition (that means using less than 4π solid angle) results in back projection artifacts in a reconstruction. For example, the intersecting spherical surfaces are seen as arcs in a section image.

In this study we developed an algorithm that reduces back projection artifacts and associated blur in three-dimensional optoacoustic images. We use an iterative method that was adapted from deconvolution techniques known from other kinds of inverse problems in fields like microscopy or spectroscopy. The algorithm uses two models:

(1) An accurate model for the forward problem, describing the generation and propagation of optoacoustic waves from an arbitrary distribution of absorbed energy and the detection of signals in an array of point detectors.
(2) A model for the inverse problem, using radial back projection of velocity potential signals as an estimate for the source distribution.

The forward and inverse models are used iteratively to obtain an optimal reconstruction. The idea is to use signals calculated at the detector positions in the array from the first image estimate, which is the result of a radial back projection of the measured signals. The calculated signals are compared with the measured signals and the difference is used to improve the reconstruction. Details of the algorithm and the forward and inverse models are presented in the next section. The other sections show a simulation with a known source distribution and an experiment demonstrating high resolution imaging of two absorbing spheres.

2. IMAGE RECONSTRUCTION ALGORITHM

The source of the optoacoustic wave is the laser-generated distribution of absorbed energy density $W(\mathbf{r'})$. Here, the primed coordinates refer to a location in the source volume, whereas the detector positions are $\mathbf{r}_i$, where the subscript denotes the number of the detector in the array. A solution of the thermoelastic wave equation that describes the production of the optoacoustic wave can be found by calculating the integral [3,6]

$$\Phi(\mathbf{r}_i, t) = \frac{\beta}{4\pi C_p} \frac{1}{t} \iint_{|\mathbf{r}' - \mathbf{r}_i| = ct} W(\mathbf{r}')\, dS, \tag{1}$$

where Φ is the velocity potential, β the thermal expansion coefficient, ρ the density, C_p the specific heat capacity at constant pressure and dS the surface element on a sphere around the point $\mathbf{r}_i$. The integration has to be performed on the surface of a sphere with radius $|\mathbf{r}' - \mathbf{r}_i| = ct$. The velocity potential is related to the particle velocity $\mathbf{v}$ by $\mathbf{v} = \mathrm{grad}\,\Phi$ and to the acoustic pressure p by

$$p(\mathbf{r}, t) = -\rho \frac{\partial \Phi}{\partial t}. \tag{2}$$

For an abbreviated description of the algorithm we will use a short form of (1), introducing an operator A that describes the generation of a set of velocity potentials Φ from the laser-generated energy distribution W,

$$\Phi = AW. \tag{3}$$

For the computations of acoustic signals we use a discrete form of Eq.(1), where the integral is replaced by a sum over a finite number of point sources. The result is a two-dimensional array Φ_{ik} with i being the position in the array and k the time index of the temporally sampled signal. Since the discretization produces noise, in a further step the result is convolved with a temporal Gaussian function $\exp[-(2t/t_{prop})^2]$, where t_{prop} is the average propagation time of the acoustic wave through a

volume element, $t_{prop} = (\Delta x+\Delta y+\Delta z)/3c$. To generate an image estimate the velocity potential is back projected into the source volume using

$$I(\mathbf{r}) = \frac{4}{\Omega}\frac{C_p}{} \sum_i t(\mathbf{r}_i, t = |\mathbf{r}_i - \mathbf{r}|/c)\, w_i . \tag{4}$$

The value of t, which according to (1) is proportional to the integral of the source distribution over a spherical surface, is in (4) distributed over points on the same area, weighted with a factor w_i. This weighting factor describes the detector directivity and may also be used to correct different sensitivities of the individual detectors of the array. For the directivity we used $\cos\theta$, where θ is the angle between vector $\mathbf{r}' - \mathbf{r}$ and the normal to the detector plane. Since detectors measure acoustic pressure, p is obtained from integrating p over time according to Eq.(2). Again we will use a symbolic form of (4), introducing a back projection operator B that transforms velocity potential signals into an image,

$$I = B\Phi . \tag{5}$$

In the algorithm that was adapted from van Cittert [7,8] new signals $\Phi^{1)}$ are calculated from the reconstructed image using Eq.(1) and the residual $\Phi - \Phi^{1)}$ is back projected and added to I. Subsequent iterations are described by

$$\begin{aligned} \Phi^{(n)} &= K \cdot AI^{(n)} \\ I^{(n+1)} &= I^{(n)} + B(\Phi - \Phi^{(n)}) \end{aligned} \tag{6}$$

The factor K normalizes $\Phi^{n)}$ in a way that energy is conserved. From Eq. (1) the following relation can be derived between the total absorbed energy Q in the source and each of the measured velocity potential signals (or acoustic pressure signals with (3))

$$Q = \iiint W\, dV = \frac{4\pi c\, C_p}{\Omega} \int t\, \Phi(\mathbf{r}_i, t)\, dt \tag{7}$$

In other words the integral over $t\Phi(\mathbf{r}_i,t)$ represents the total absorbed energy. To make the energy content in Φ and $\Phi^{n)}$ equal the normalization factor has to be

$$K = \int t\, \Phi(\mathbf{r}_i, t)\, dt \Big/ \int t\, \Phi^{(n)}(\mathbf{r}_i, t)_{us}\, dt , \tag{8}$$

where $\Phi(\mathbf{r}_i,t)_{us}$ is the velocity potential before normalization. The normalization does not require knowledge of the absorbed energy. However, using a calibrated detector array the absorbed energy can be calculated from (7). After each iteration only image values greater than zero are kept. This non-negativity constraint is justified because the absorbed energy cannot be negative. To monitor the convergence of the algorithm an error is calculated after each iteration

$$err^{(n)} = \sum_i \sum_j (\Phi_{ik} - \Phi_{ik}^{(n)})^2 , \tag{9}$$

using indices i and k for detector number and time, respectively. As a condition for terminating the iterations we used

$$\frac{err_{\Phi}^{(n+1)} - err_{\Phi}^{(n)}}{err_{\Phi}^{(1)}} < 0.01, \tag{10}$$

which stopped the algorithm when the improvement per iteration became smaller than 1% of the initial error. To convert image data into absolute energy density the reconstruction can be normalized with the total energy Q,

$$I_{abs}^{(n)} = I^{(n)} \frac{Q}{\int I^{(n)}\, dV}, \tag{11}$$

where Q is calculated from (7). Here the condition is used that the volume integral over $I_{abs}^{(n)}$ must equal the total absorbed energy.

3. SIMULATION

A simulation with a known source distribution was performed to test the reconstruction algorithm. The source consisted of spherically symmetric Gaussian functions with an $1/e$ radius of a = 0.2 mm,

$$W(\mathbf{r}) = \exp(-(\mathbf{r} - \mathbf{r}_c)^2 / a^2), \tag{12}$$

where $\mathbf{r}_c$ is the position of the center. Two sources (hereafter referred to as "spheres") were located in a cube with a size of 2 x 2 x 2 mm^3, at the Cartesian coordinates $\mathbf{r}_{c1}$ = (1.5, 1, 0.8) mm and $\mathbf{r}_{c2}$ = (0.5, 1, 1.3) mm. Signals were calculated for an array of 3 x 3 detectors in a plane. The source cube was divided into a grid of 40 x 40 x 40 points. The arrangement of sources and detector array is schematically shown in Fig.1. The top row of Fig.2 shows a section image of W through the centers of the two spheres and a representative velocity potential signal Φ calculated for one of the detector positions. In the second row is the first image estimate $I^{(1)}$ and an overlay of a signal $\Phi^{(1)}$ calculated from $I^{(1)}$ and the residual Φ - $\Phi^{(1)}$ that is back projected and added to $I^{(1)}$ to generate $I^{(2)}$. The last row shows the final reconstruction $I^{(12)}$ and the error as a function of the number of iterations. All images are scaled to use the complete range of gray levels. The intensity bars, however, show the absolute energy density after normalization with Eq.(11). Although the spheres 1 and 2 are still visible in $I^{(1)}$ their resolution is strongly diminished. This also affects the signal $\Phi^{(1)}$, where the separation of the two peaks is much worse than in the original measured signal. This gives rise to the negative parts in the residual and its correcting effect in the subsequent back projection. In the final reconstruction the resolution of the spheres is much better than in the first back projection. The improvement can also be seen in the error graph where a reduction of the error to about 40% of its initial value is achieved.

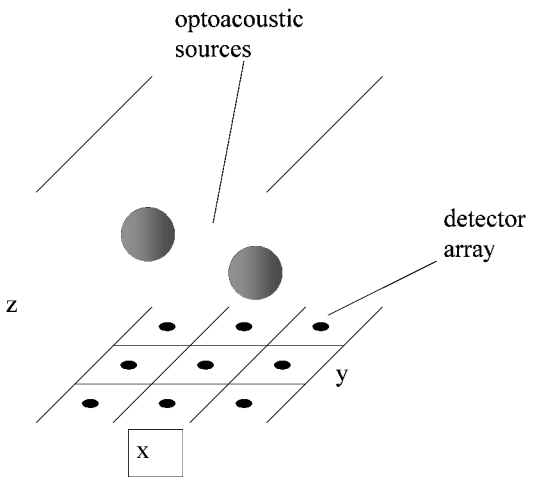

Fig.1 Arrangement of detector array and spherical optoacoustic sources for the simulation. 9 array elements were placed in the bottom plane of a 2 x 2 x 2 mm^3 cube.

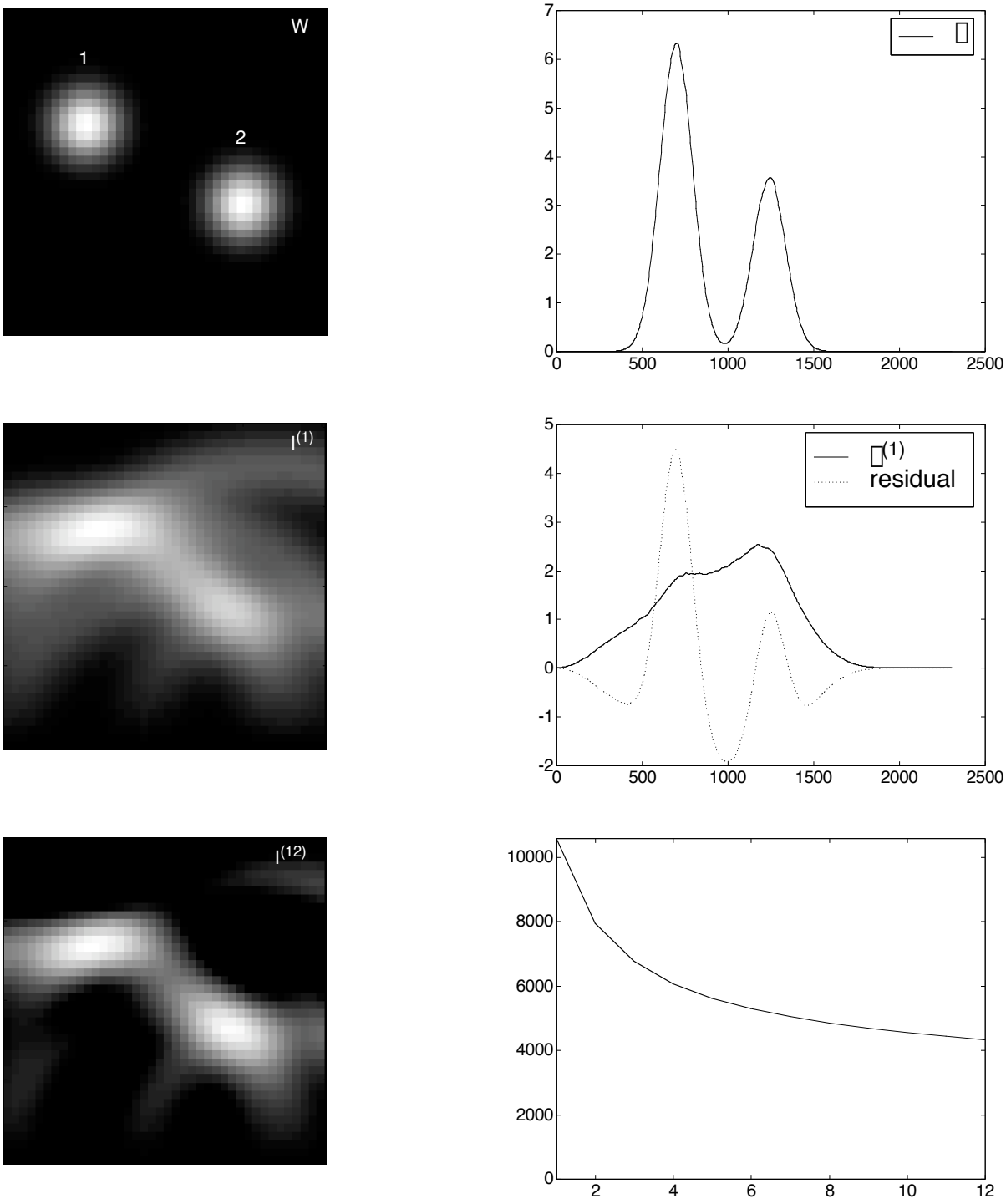

Fig.2 Results of simulation. First row: Original source distribution W and representative signal Φ at one of the 9 detector positions. Second row: Image $I^{(1)}$ and velocity potential $\Phi^{(1)}$ calculated from $I^{(1)}$ together with residual $\Phi - \Phi^{(1)}$. Third row: Final reconstruction $I^{(12)}$ and error as a function of the number of iterations.

4. EXPERIMENT

Absorbing sources in an optically clear environment were imaged using the experimental setup shown in Fig.3. Two spheres made of acrylamide gel with added absorber (Direct Red 81, Sigma Chemical) were placed on a thin plastic film and were surrounded by clear mineral oil. The oil prevented the dye from diffusing out of the spheres. The diameters of the spheres were 1.2 and 1.5 mm, respectively and the distance between the centers was 2.15 mm. The absorption coefficient of the gel was $\mu_a = 60$ cm^{-1}. A 1 mm diameter optical fiber was used to irradiate the spheres from above. As a laser source we used a frequency-doubled, Q-switched Nd:YAG laser with a pulse duration of 5 ns operating at a wavelength of 532 nm. The laser pulse energy was 5 mJ and the laser spot diameter was 4 mm, giving an incident radiant exposure of $H_0 = 0.04$ J/cm^2. With an optical absorption depth $1/\mu_a$ of 170 µm both spheres were optically thick, and therefore only a thin layer facing the incident laser pulse was heated. The maximum energy density in the heated layer was $W_0 = \mu_a H_0 = 2.4$ J/cm^3. For the recording of acoustic signals we used an optical detector [9]. A continuous HeNe probe beam was focused to an elliptical spot with principal diameters of 120 and 250 µm on the interface of a glass prism and a water layer. The layer separated the glass prism from the plastic film carrying the gel spheres and had a thickness of 3 mm. An acoustic wave being incident on the glass surface from the water layer slightly changed the relative optical refractive index between the two media, thereby varying the Fresnel reflectance of the interface. This caused modulations of the probe beam intensity that were detected with a fast photodiode. The signals from the photodiode were amplified and recorded on a digital storage oscilloscope. Choosing an incident angle of the probe beam slightly smaller than the critical angle of total internal reflection of the glass-water interface maximized the sensitivity of the detector. The undisturbed optical reflectance at the prism water interface was 0.8. Calibrating the detector using a procedure based on the Fresnel formula and the change of refractive index with pressure, $dn/dp = 1.35 \times 10^{-5}$ bar^{-1} yielded a sensitivity of 0.6% modulation per bar of pressure. The overall sensitivity of the system taking into account the response of the photodiode and the gain of the amplifier was 1 mV/bar. The noise level of averaged signals (over 32 sweeps) was about 20 µV or 20 mbar. To simulate a detector array, the single detector point was scanned over a grid of 3 x 3 points in a plane, with a grid size of 1 mm in x-direction and of 1.5 mm in y-direction.

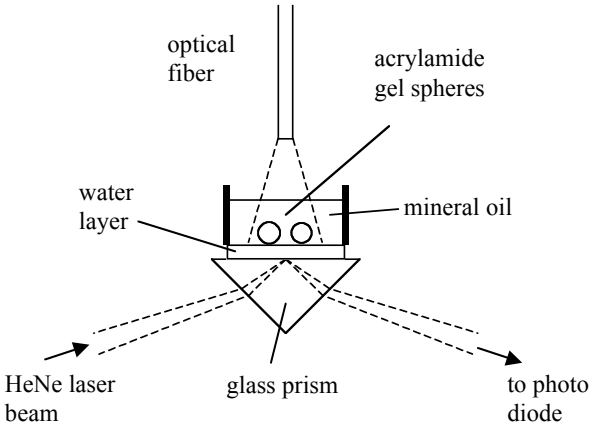

Fig.3 Experimental setup for optoacoustic imaging of two absorbing spheres embedded in mineral oil. The HeNe laser beam is modulated by the pressure waves crossing the water-glass interface. Mineral oil and water layer are separated by a thin plastic film.

5. RESULTS

A typical acoustic pressure signal and the corresponding velocity potential are shown in Fig.4. Although the pressure signal is quite noisy the velocity potential clearly shows the two peaks coming from the spheres. Figure 5 shows two sections of the reconstructed volume (size 4 x 6 x 4 mm^3), one parallel to the y-z-plane and one parallel to the x-y-plane. For each plane, the figure depicts the first order reconstruction, $I^{(1)}$ and the final reconstruction $I^{(11)}$ after 11 iterations, when the algorithm was stopped according to the condition in Eq.(10). Figure 6 displays the error as a function of the number of iterations. Back projection artifacts are visible as arcs in the y-z-section and as blur in the x-y-section of $I^{(1)}$. These artifacts are strongly reduced after the iterations. The values in the gray level bars of Fig.5 are absorbed energy density in units of J/cm^3. They were obtained using the normalization described in Eq.(11). The total absorbed energy was calculated from the measured acoustic signals using Eq. (7), which gave an average value of 1.5 mJ. Due to less spreading of energy in back projection spheres the maximum energy density increased by a factor of 8 between $I^{(1)}$ and $I^{(11)}$ but did not reach the predicted value of 2.4 J/cm^3.

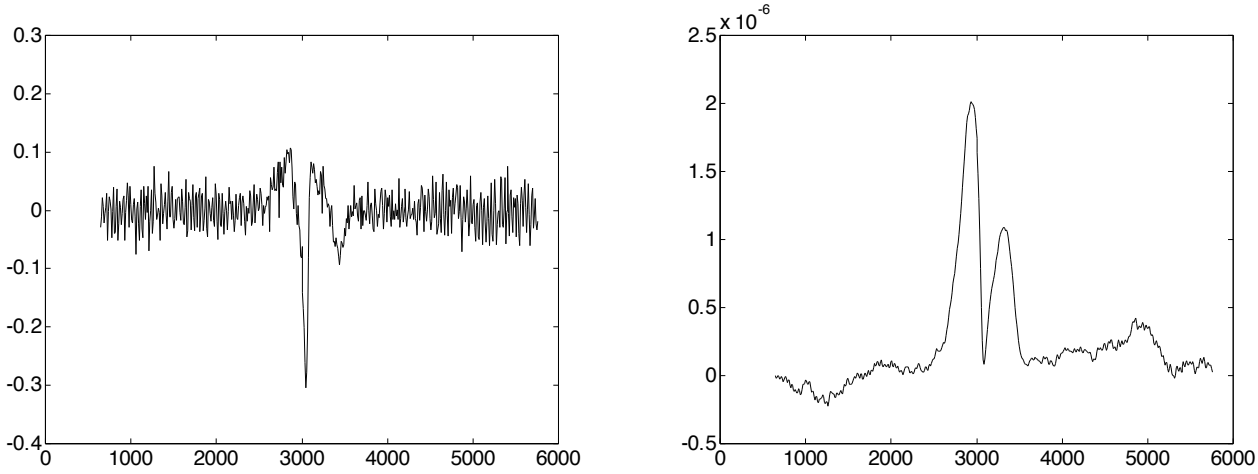

Fig.4 Acoustic pressure (left) and inverted velocity potential (right) signals measured at one of the detector positions with the optical detector.

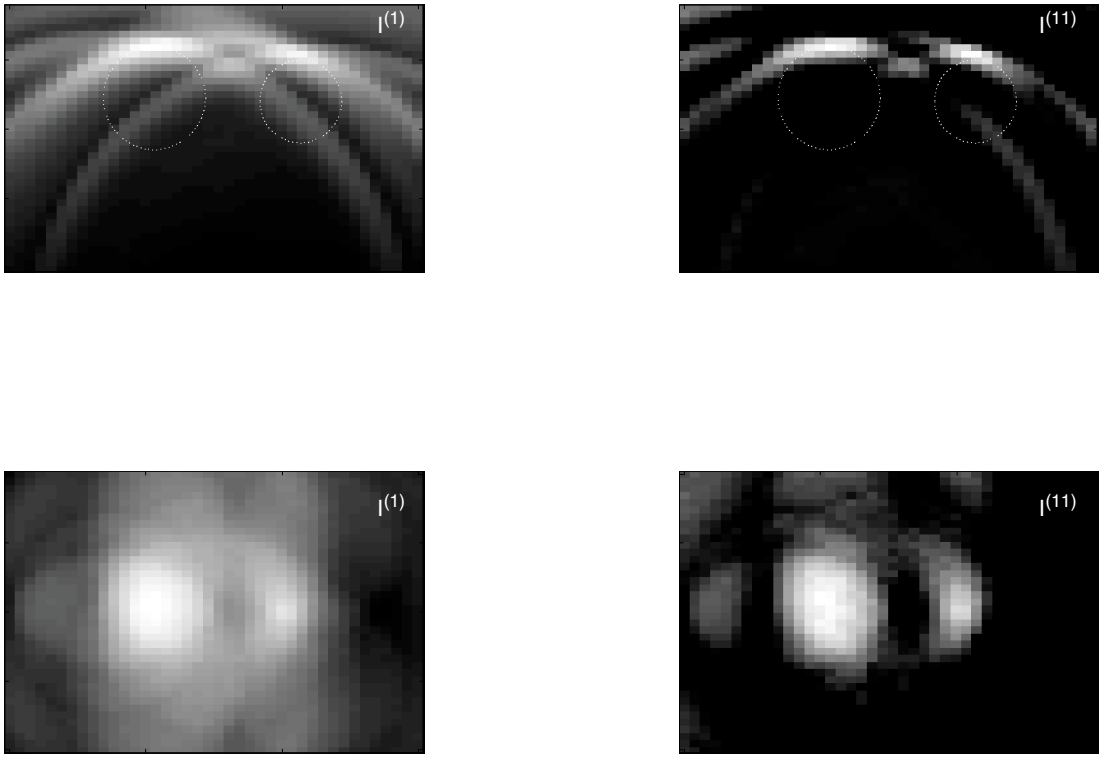

Fig.5 Results of experimental image reconstruction. Displayed are sections in a *y*-*z*-plane (first row) and in a *x*-*y*-plane (second row). The left column contains sections of the first estimate $I^{(1)}$ and the right column of the final reconstruction $I^{(11)}$. Values in the gray level bar are energy density in J/cm^3. The circles in the images indicate the positions of the spheres.

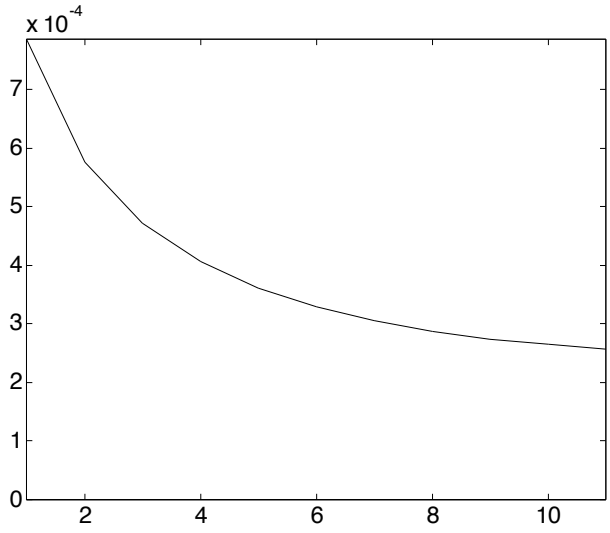

Fig.6 Error as a function of the number of iterations in the experiment.

6. DISCUSSION

We have presented an iterative algorithm for reconstruction of the absorbed energy distribution after irradiating a sample with a ns-laser pulse. The optoacoustic waves generated in the sample are measured with an ultrasound detector array. After several iterations the result of the reconstruction was significantly improved compared to simple radial back projection. The most striking improvement was a reduction of back projection artifacts such as arcs. The improvement of the first image estimate can be regarded as a three-dimensional deconvolution problem, where the original distribution is smeared by the signal acquisition and back projection procedures with a characteristic response function or point spread function (PSF) of the imaging system. In contrast to many other deconvolution problems where the PSF is spatially invariant, the radial back projection used in optoacoustic imaging produces a PSF that is dependent on the location in the source volume. A simple inverse filtering approach is therefore not applicable.

Using the relation between total absorbed energy and measured pressure signal (7) and applying the normalization in Eq.(11) it was possible to calculate the absolute three-dimensional distribution of absorbed energy. It turned out, however, that although the iterations increased the source strength, the resulting maxima of the reconstructed distributions were still too low compared with the original. This was due to some residual spreading of energy over back projection spheres. Since the normalization requires the volume integral over the reconstruction to be equal to the total absorbed energy, this slight residual spreading of energy caused the drastic reduction of reconstructed energy density maxima.

The relative source strengths could be corrected quite well. In the simulation the two spherical sources had an original maximum of 1. The simple radial back projection produced a wrong relative source strength distribution with maxima of 0.047 for source 1 and 0.037 for source 2. After 12 iterations the maxima of both sources were equal and amounted to 0.12. This is the main reason why the iterative approach works better than simple thresholding. Applying a threshold to the first estimate would have reduced back projection artifacts but would also have increased the discrepancy between the two sources.

Since the algorithm requires repeated calculation of the forward problem that in turn requires knowledge of a three-dimensional source distribution it can only be applied to reconstruct the whole three-dimensional image, not only a two-dimensional section. This makes the algorithm computationally intensive. For example, calculation of one signal from a 40 x 40 x 40 grid required about 6 seconds (G4 Power PC, Apple Computers). The same time was needed to back project one signal. With a 9 detector array one iteration was accomplished in little less than 2 minutes and the total reconstruction took about 20 minutes.

7. CONCLUSION

Optoacoustic images reconstructed from ultrasound array signals can be significantly improved with an iterative algorithm. Although the computation time is increased compared to a one-step reconstruction the iterative approach may save measurement time because it maximizes the information taken from the acquired signals.

ACKNOWLEDGMENTS

G. Paltauf is supported by the Austrian Programme for Advanced Research and Technology (APART) of the Austrian Academy of Sciences.

REFERENCES

1. C.G.A. Hoelen, F.F.M. de Mul, R. Pongers, and A. Dekker, "Three-dimensional photoacoustic imaging of blood vessels in tissue," Opt. Lett. **23**, pp. 648-650, 1998.
2. V.A. Andreev, A.A. Karabutov, S.V. Solomatin, E.V. Savateeva, V. Aleynikov, Y.V. Zhulina, R.D. Fleming, and A.A. Oraevsky, "Opto-acoustic tomography of breast cancer with arc-array-transducer," in *Biomedical Optoacoustics*, edited by A.A. Oraevsky, Proc. SPIE 3916, pp. 36-47, SPIE, Bellingham, 2000.
3. R.A. Kruger, W.L. Kise, K.D. Miller, H.E. Reynolds, D.R. Reinicke, G.A. Kruger, and P.J. Hofacker, "Thermoacoustic CT: Imaging principles," in *Biomedical Optoacoustics*, edited by A.A. Oraevsky, Proc. SPIE 3916, pp. 150-159, SPIE, Bellinghan, 2000.
4. G. Paltauf, H. Schmidt-Kloiber, K.P. Koestli, M. Frenz, and H.P. Weber, "Optoacoustic imaging using two-dimensional ultrasonic detection," in *Biomedical Optoacoustics*, edited by A.A. Oraevsky, Proc. SPIE 3916, pp. 240-248, SPIE, Bellingham, 2000.
5. P. Liu, "The P-Transform and photoacoustic image reconstruction," Phys. Med. Biol. **43**, pp. 667-674, 1998.
6. G. Paltauf, H. Schmidt-Kloiber, and M. Frenz, "Photoacoustic waves excited in liquids by fiber-transmitted laser pulses," J. Acoust. Soc. Am. **104**, pp. 890-897, 1998.
7. P.H. van Cittert, "Zum Einfluß der Spaltbreite auf die Intensitätsverteilung in Spektrallinien," Zeitschr. f. Physik **69**, pp. 298-308, 1931.
8. P.A. Jansson, "Method for determining the response function of a high-resolution infrared spectrometer," J. Opt. Soc. Am. **60**, pp. 184-191, 1970.
9. G. Paltauf and H. Schmidt-Kloiber, "Measurement of laser-induced acoustic waves with a calibrated optical transducer," J. Appl. Phys. **82**, pp. 1525-1531, 1997.